




Using multiple composite fingerprints to quantify source contributions and uncertainties in an arid region

Baicheng Niu^{1,2} · Xunchang (John) Zhang³ · Jianjun Qu¹ · Benli Liu¹  · Joel Homan³ · Lihai Tan¹ · Zhishan An¹

Received: 1 March 2019 / Accepted: 29 July 2019 / Published online: 16 August 2019
© Springer-Verlag GmbH Germany, part of Springer Nature 2019

Abstract

Purpose Developing targeted protection measures at a watershed scale requires spatially distributed information of sediment sources. Therefore, the objectives of this study are to (1) test and evaluate the ability of multiple composite fingerprints (MCF) to quantify sediment provenance using multiple particle size classes in an arid region; (2) quantify uncertainty of the estimated proportional contributions of sediment sources; and (3) provide decision support information for sediment control in the Danghe Reservoir Watershed.

Materials and methods In total, 66 samples were collected from north alluvial fan, south alluvial fan, and high mountains, and all samples were divided into six particle size groups. A multistep test was used to remove the tracers that were non-conservative, unable to differentiate sources, or highly variable within a source. Based on geochemical properties of distributed source samples and a linear mixing model, a MCF method with multiple particle size tracking was used to estimate proportions of three potential source contributions. More importantly, the uncertainty of sediment source contributions was quantified using the Gaussian first-order approximation.

Results and discussion The results showed that the MCF method with multiple particle size tracking could obtain relatively accurate estimates of the contributions with an overall mean absolute relative error of 3.5% and a relatively narrow 95% confidence interval. The major contributions were consistently coming from the high mountains for all six particle groups. During these runoff events, the overall estimated mean proportions were 49.0%, 26.5%, and 24.5% from the high mountains, south alluvial fan, and north alluvial fan, respectively. Furthermore, the Gaussian first-order approximation revealed that more than 60% of the total uncertainty contribution was a byproduct of the downstream sediment mixture, while each individual sediment source produced less than 15% of the absolute uncertainty.

Conclusions Acquiring watershed scale sediment source information is challenging and the MCF method proved accurate. A majority of the contribution uncertainties were associated with the downstream sediment mixture, which is because the sediment sink inherited both spatial and temporal variations of all contributing sources. Consequently, a larger sample size is recommended for sediment mixtures, compared to each sediment source, in order to increase the accuracy of the source proportion estimation.

Keywords Arid region · Multiple composite fingerprints · Sediment provenance · Uncertainty analysis

Responsible editor: Alexander Koiter

Electronic supplementary material The online version of this article (<https://doi.org/10.1007/s11368-019-02424-1>) contains supplementary material, which is available to authorized users.

✉ Benli Liu
liubenli@lzb.ac.cn

² University of Chinese Academy of Sciences, Beijing 100049, China

³ Grazinglands Research Laboratory, Agricultural Research Service, United States Department of Agriculture, El Reno, OK 73036, USA

¹ Dunhuang Gobi Desert Research Station, Key Laboratory of Desert and Desertification, Northwest Institute of Eco-Environment and Resources, Chinese Academy of Sciences, Lanzhou 730000, China

1 Introduction

Soil erosion exerts significant impacts on societal development. Severe soil erosion leads to soil nutrient loss, water quality degradation, river siltation, and reservoir capacity loss (Liebe et al. 2005; Khaba and Griffiths 2017; Emamgholizadeh et al. 2018; Gonzalez 2018). Quantifying the sources of sediments is critical for developing appropriate and site-specific conservation measures that effectively control soil erosion within a watershed (Zhang et al. 2016a). Information on sediment sources is unfortunately limited, because most types of soil erosion and transport processes are spatially complex and difficult to measure at a watershed scale. Measuring the contributions from different sources of sediment is primarily completed using three methods. The first is a conventional method, such as erosion pins (Davis and Gregory 1994; Bak et al. 2013; Boardman et al. 2015), mapping (Cao and Coote 1993), remote sensing (Thakur et al. 2012), and photogrammetry (Barker et al. 1997), but these approaches are mainly used in a relatively small watershed with the same type of dominant soil erosion. Using the conventional method, it is almost impossible to directly measure multiple erosion types within a watershed. The second is the fingerprinting technique, which can estimate sediment source contributions using various natural sediment tracers, or fingerprints, by linear mixing models (Collins et al. 1996; Krause et al. 2003; Stone et al. 2014; Zhang et al. 2016a). The fingerprinting method is suitable for any watershed size and complexity, so long as distinct fingerprint properties exist in different sediment sources (Zhang et al. 2016a). The third is the application of artificial tracers (Haddadchi et al. 2014; Zhang et al. 2017), which is mainly suitable for small watersheds or erosion plots but not for large watersheds.

In early fingerprinting method studies, typically a single fingerprint property was used to identify a sediment source (Lance et al. 1986; Roo 1991; Olley et al. 1993). When collected sediment has more than two sources or the spatial variability of the source is large, the discrimination of a single property is limited. For more complex scenarios, a composite fingerprint with multiple properties of distinct types can be used to identify sediment sources, which could vastly improve the partitioning of a sediment source (Collins et al. 1997, 1998, 2010; Koiter et al. 2013; Laceby and Olley 2015; Zhou et al. 2016). An “optimal” composite fingerprint that was selected to obtain maximized discriminant ability with minimum tracers was proposed by Collins et al. (1997) and widely used in the literature. However, Zhang and Liu (2016) found there was weak relationship between the ability of a tracer in distinguishing sources and its power in estimating contributions of the sources to sediment mixtures (sink) if the tracer is non-conservative during transport. However, quantifying the conservativeness of a tracer in a watershed is not an easy task, if not impossible, requiring enormous

amounts of sampling and chemical analyses of different particle size classes. To circumvent this weakness, an approach using multiple composite fingerprints was proposed by Zhang and Liu (2016). The new approach uses a maximum number of composite fingerprints composed of non-contradictory tracers to obtain multiple analytical or numerical solutions, and uses the mean estimates of the multiple composite fingerprints as source contributions. From a statistical point of view, the contributions of different sediment sources averaged over multiple composite fingerprints are more likely to be closer to the real values than any estimates using a composite fingerprint alone, when multiple contribution proportions are approximately normally distributed. The method has been verified by contrasting with other methods (Zhang and Liu 2016), and further compared to the results from ^{137}Cs analysis with greater confidence (Zhang et al. 2016b). Some studies showed that the method of multiple composite fingerprints could obtain reasonable results in watersheds dominated with eolian or water erosion (Liu et al. 2016; Zhang et al. 2016a).

In previous studies, the particle size fraction of < 0.063 mm is most commonly used to identify source contributions within a watershed. Furthermore, particle size correction factors are often used in addition to account for any remaining difference in grain size between the source and the downstream sediment (Collins et al. 1998; Walling 2005; Devereux et al. 2010; Hancock and Revill 2013; Palazon and Navas 2017; Koiter et al. 2018). Other particle size fractions are also used, such as < 0.002 mm fraction (Gingele and Deckker 2005), < 0.004 mm fraction (Wallbrink et al. 2003), < 0.010 mm fraction (Wilkinson et al. 2013; Laceby and Olley 2015), < 0.053 mm fraction (Zhang and Liu 2016), < 0.25 mm fraction (Evrard et al. 2013), as well as multiple particle size groups (Haddadchi et al. 2015). The multiple particle size tracking has distinct advantages to identify sediment sources, but is more time consuming and costly (Collins et al. 2017). The sediment sources of the different particle size fractions may have different transport modes, and also have different negative effects on a catchment network requiring different treatment strategies. Therefore, based on the particular situation present in a watershed, the particle size fraction used in identifying main sediment source needs to be selected carefully.

When using fingerprint technology to identify sediment sources, providing estimated uncertainty of source contributions allows for more informed decisions on sediment and water management (Minella et al. 2008). Thus, it is critical to pay more attention to uncertainty assessment (Walling 2013). In recent years, both statistical and analytical methods were used to assess uncertainty. The former includes Monte Carlo simulations and Bayesian uncertainty framework, and the latter includes Gaussian first-order approximations. Monte Carlo simulations are mainly used to repeatedly simulate, with random sampling, the distributions of each input tracer in sediment mixtures and from each source, and to generate the

probability distribution for the output (Motha et al. 2003; Nagle et al. 2007; Collins et al. 2010; McKinley et al. 2013; Stone et al. 2014; Zhang and Liu 2016). Bayesian uncertainty frameworks are used to simulate probability distributions of estimated source proportions (Koiter et al. 2013; Stewart et al. 2015). In most studies, contributions of different sediment sources are calculated using average values of sediment sources and sediment mixtures in the mixing model, and the use of the averages is an important source of uncertainty in the source contribution estimates (Lamba et al. 2015). If the uncertainty band is not explicitly estimated, this situation often causes false certainty on estimated proportions. The Gaussian first-order approximation can be readily used to obtain uncertainty contributions from each potential source and mixture for the mean contribution of a certain sediment source; however, the method is rarely applied in the literature.

In the current investigation, a multiple composite fingerprinting method was used to quantify sediment source contributions in the upper reaches of the Danghe Watershed in Northwest China. Because both water and wind erosion predominate the watershed and as a result of sediment sorting during transport being severe, tracking multiple particle size groups was adopted to minimize estimation errors caused by sediment sorting and the Gaussian first-order approximation to quantify uncertainty of the mean source contributions.

2 Materials and methods

2.1 Study watershed

The area of investigation is within the mountainous region of the Danghe Reservoir Watershed located in Northwest China along the western Hexi Corridor. The Danghe watershed has a drainage area approximately 16,970 km² and is largely composed of dunes, Gobi desert, and mountains. The mountain region comprises a majority of the overall watershed area (15,281 km²) and is the primary sediment source of the Danghe Reservoir (Niu et al. 2019). Thus, the mountain region was evaluated more closely as a focused area of interest for this investigation (Fig. 1c). To further partition the potential sediment sources, the mountain region was subdivided into north and south alluvial fans and high mountains (Fig. 1b).

The alluvial fans are predominantly located on the piedmont of the mountains between 1800 and 2800 m above mean sea level. The alluvial fans located north of the Danghe River encompass a drainage area approximately 728 km², while alluvial fans to the south incorporate 228 km². The ground surface of the north alluvial fan is primarily a composite of hard rocks that mainly include quartz diorite, siliceous rock, and limestone, and they are weathering resistant. However, the south alluvial fan is mainly a composite of orange-red clastic

rocks and a small amount of the exposed bedrocks (Proterozoic Sinian), and the former is more easily weathered and eroded than the latter. Furthermore, compared to the south alluvial fan, the north alluvial fan has an abundance of anthropogenic activities, such as agriculture and urban development. The surface materials are significantly different between the two alluvial fans.

The high mountains, defined as the area above 2800 m mean sea level, occupy a significant portion (~93.7%) of the research area with an area of 14,325 km². The high mountains are characterized by rough steep terrains and alpine canyons under complex geomorphologic patterns. The geological composition of the mountains is complex with many types of rocks, such as flash feldspar, quartz diorite, monzonitic granite, mudstone, river and lake facies clastic rocks, sand, gravel, and silty clay. Therefore, the sediment mixture of mountains should be different from the alluvial fans.

The average annual rainfall is about 86–280 mm in this research area. The average annual rainfall amounts are different between alluvial fans and high mountains. Because the annual rainfall increases by 8–12 mm as the altitude increases by 100 m, the high mountains have greater amounts of precipitation than the piedmont fans. To compound the situation further, precipitation events in the high mountains tend to be more intense due to more active convection, often resulting in flash floods.

2.2 Sample collection and processing

The Danghe Reservoir Watershed upstream mountain region, which includes the north alluvial fan, south alluvial fan, and high mountains, was identified as potential sediment sources according to their associated geomorphic terrains. At the downstream boundary of the upstream mountain region, a short reach in the main river channel was selected to collect sediment samples (Fig. 1d). The idea is that the sediment within the downstream river channel is a combination or mixture of the three potential upstream sediment sources. The downstream river channel sediments were obtained using sediment collection traps (Phillips and Gregg 2001; Zhang and Liu 2016). The traps were constructed from stainless steel pipes (14 cm i.d., and 60 cm long) with outward pointing funnels mounted to each end (a 3-cm opening upstream and a 2-cm opening downstream). Three traps were anchored to the riverbed along a cross-section of the downstream river channel (Fig. 1e). The traps were retrieved and emptied of newly collected sediment on four separate occasions (5/Sept./2016, 18/July/2017, 2/Aug./2017, and 20/March/2018) after flood waters receded. The sediment samples were collected after two heavy rains with large floods on 18/July/2017 (runoff 11.18 million m³/event; rainfall 10.6 mm/event) and on 2/Aug./2017 (runoff 5.61 million m³/event; rainfall 7 mm/event), as well as after two small runoff events on

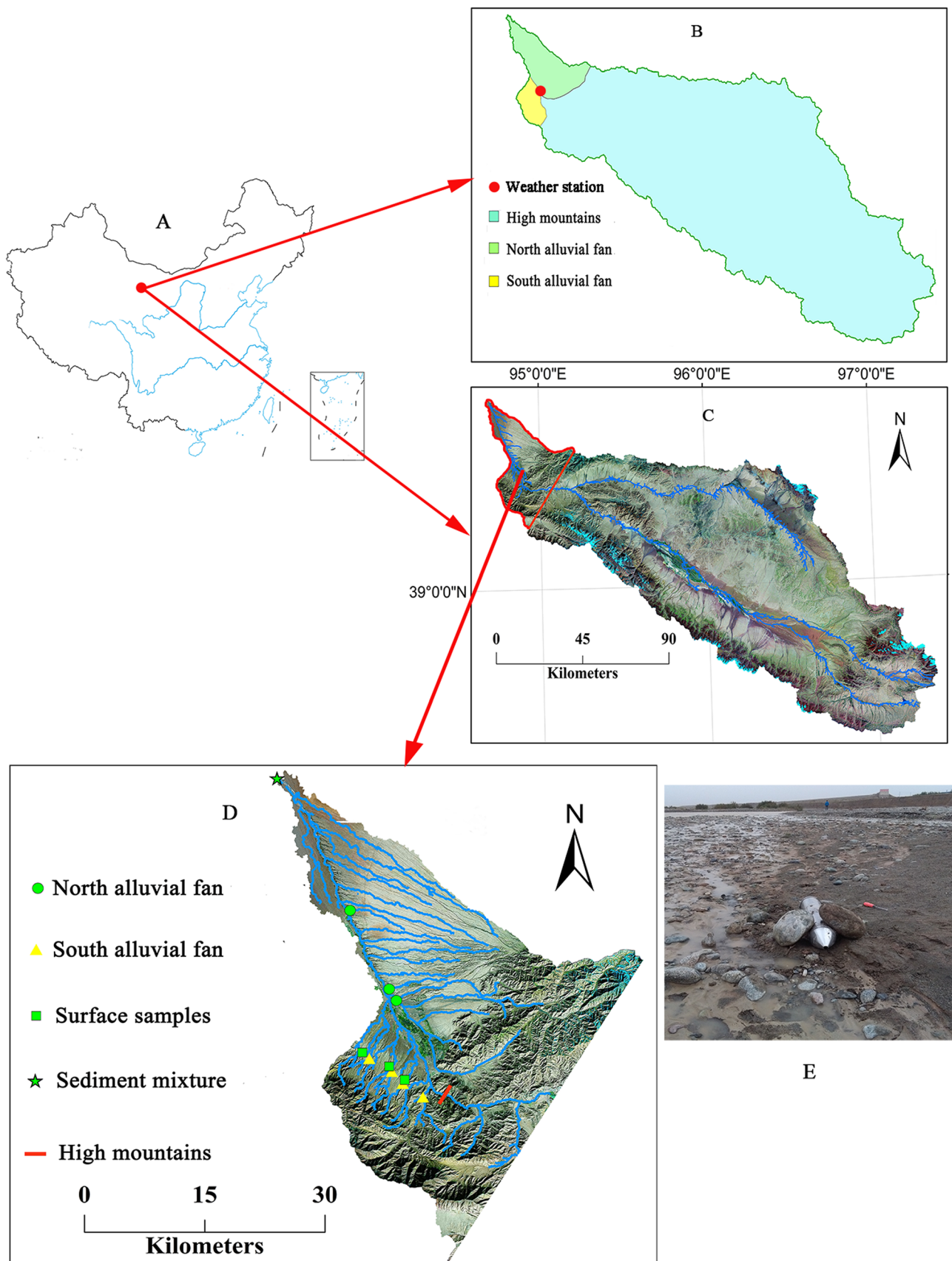


Fig. 1 Location of the study area and sampling sites (A: Map of China; B: Source area classification; C: Watershed map of the study area; D: Sampling sites; E: Sediment trap)

5/Sept./2016 (rainfall 4.3 mm/event) and 20/March/2018 (snow melt). In conjunction with the sediment traps, newly deposited riverbed surface sediment was also collected along the channel cross-section using a small stainless steel spade after flood receded. The surface sediment samples consisted of five random sampling locations, each of which included a composite of 5–10 subsamples within a single sampling area of roughly 4 m². In total, nine samples were collected.

Limited accessibility to the high mountains presented a particular challenge for collecting distributed samples that represent the sediment properties of the entire upper domain. Therefore, a single channel section, one which controls the drainage of the high mountains, was selected to collect lumped riverbed surface sediment samples (Fig. 1). The high mountain samples were acquired after the two heavy rainfall-runoff events (18/July/2017 and 2/Aug./2017) and consisted of eight samples collected from the river channel following the spade grab sampling procedure described in the preceding paragraph. A total of eight riverbed surface samples represented the high mountain sediment (Table 1).

The north and south alluvial fans regions, though much smaller than the high mountains, have many tributaries, some of which are difficult to access. Thus, readily reachable tributary channels representative of typical surface rocks/materials and geomorphic units were chosen from both north and south alluvial fans to characterize the sediment from their respective areas (Fig. 1). At the downstream boundary of selected tributaries, which included three in the northern alluvial fan and four in the south alluvial fan, between 5 and 7 riverbed surface sediment grab samples were collected after the two heavy rainfall-runoff events (18/July/2017 and 2/Aug./2017) (Fig. 1). The sampling procedures remained consistent with the protocols described above and in total 19 samples were collected from the north alluvial fan tributaries and 21 samples from the south alluvial fan tributaries (Table 1). Additionally, nine soil samples were collected from the surface (0–2 cm) of the south alluvial fan where erosion was occurring. Jointly, a sum of 30 sediment samples were obtained from the south alluvial fan.

In the lab, the 66 soil or sediment samples were oven-dried at 105 °C for approximately 12 h. Subsequently, the samples were separated into six particle size categories (< 0.063 mm, 0.063–0.1 mm, 0.1–0.25 mm, 0.25–0.5 mm, 0.5–1.0 mm, 1.0–2.0 mm) using an electric sieve shaker (Table 1 and [Electronic Supplementary Material](#)).

2.3 Chemical analysis

In order to perform sediment source fingerprinting or element tracing procedures, the geochemical properties of the sediment samples were analyzed. This process involved crushing all sediment samples in Table 1, including each of the six particle size groups, into powders finer than 75 μm using a

multipurpose grinder. Subsequently, 4 g of the resulting powders was pressed into 32 mm diameter pellets under 30 tons of pressure using a pressed powder pellet technique. The resulting pellets from each of the sediment samples were then entered into a fully automated sequential wavelength dispersive X-ray fluorescence spectrometer, which provided element concentrations for 30 different compounds. The chemical elements and oxide compounds analyzed included Cl, P, Ti, V, Cr, Mn, Co, Ni, Cu, Zn, Ga, As, Br, Rb, Sr, Y, Zr, Nb, Ba, La, Ce, Nd, Pb, SiO₂, Al₂O₃, Fe₂O₃, MgO, CaO, Na₂O, and K₂O. The element concentrations were in the units of μg g⁻¹, and the oxide concentrations were in percentage. The analytical precision for the macroelements is 5%, and 25% for the microelements.

2.4 Linear mixing model and Gaussian uncertainty approximation

Mathematical un-mixing models are available for the quantitative distribution of sediment provenances. For this investigation, a linear un-mixing model based on the principle of mass conservation was used to estimate the contributions of the potential sediment sources using the following equations:

$$\sum_{s=1}^m P_s \times S_{s,i} = C_i \quad (1)$$

$$\sum_{s=1}^m P_s = 1 \text{ and } 0 \leq P_s \leq 1 \quad (2)$$

where P_s is the proportional contribution from a certain size group of source s ; $S_{s,i}$ and C_i are the mean concentrations of fingerprint property i in source s and sediments, respectively; and m is the number of sources. Only $(m - 1)$ tracers are needed to analytically estimate the proportions of m sources under the constraint of $0 \leq P_s \leq 1$ in Eq. (2). For the three sediment sources (north alluvial fan, south alluvial fan, and high mountains), two tracers were needed to analytically solve Eqs. (1) and (2). The average concentrations of each tracer, from each of the potential sediment sources and sediment mixtures, were used in Eq. (1). Both Eqs. (1) and (2) were solved individually for each of the six particle size classes. As a result of low organic contents in the sediment samples, as well as low concentrations of organic matter in most of the chemical analyses (Table 1), no correction was applied to the samples for organic matter. Some studies have shown that the use of weighting factors for organic matter has resulted in overcorrections (Lacey and Olley 2015). Because the element analysis was carried out for each particle size, rather than for an aggregated sediment sample, differences in grain size were reduced and, therefore, no particle size correction factors were used.

If we can assume that the two tracers from the three sediment sources and the sediment mixture are independent of each other, then Gaussian first-order approximation can be

Table 1 Sample numbers for six particle size groups and the range of maximum organic matter contents (OMC, %) from sediment mixture

| Size (mm) | North alluvial fan | South alluvial fan | High mountains | Sediment mixture | OMC |
|-----------|--------------------|--------------------|----------------|------------------|------|
| < 0.063 | 19 | 30 | 8 | 9 | 0.66 |
| 0.063–0.1 | 19 | 30 | 8 | 9 | 0.60 |
| 0.1–0.25 | 19 | 30 | 8 | 9 | 0.52 |
| 0.25–0.5 | 19 | 30 | 8 | 9 | 0.60 |
| 0.5–1 | 19 | 30 | 8 | 9 | 0.47 |
| 1–2 | 18 | 29 | 7 | 9 | 0.59 |

used to calculate the variance of f_h (the same for f_n and f_s) (Phillips and Gregg 2001):

$$\begin{aligned} \sigma_{f_h}^2 = & \left(\frac{\partial f_h}{\partial C_{m_1}}\right)^2 \sigma_{C_{m_1}}^2 + \left(\frac{\partial f_h}{\partial C_{h_1}}\right)^2 \sigma_{C_{h_1}}^2 + \left(\frac{\partial f_h}{\partial C_{n_1}}\right)^2 \sigma_{C_{n_1}}^2 \\ & + \left(\frac{\partial f_h}{\partial C_{s_1}}\right)^2 \sigma_{C_{s_1}}^2 + \left(\frac{\partial f_h}{\partial C_{m_2}}\right)^2 \sigma_{C_{m_2}}^2 \\ & + \left(\frac{\partial f_h}{\partial C_{h_2}}\right)^2 \sigma_{C_{h_2}}^2 + \left(\frac{\partial f_h}{\partial C_{n_2}}\right)^2 \sigma_{C_{n_2}}^2 \\ & + \left(\frac{\partial f_h}{\partial C_{s_2}}\right)^2 \sigma_{C_{s_2}}^2 \end{aligned} \tag{3}$$

where $f_h, f_n,$ and f_s are the proportions of high mountains, north alluvial fan, and south alluvial fan. ∂f_h ($\partial f_n, \partial f_s$) is the partial derivative of f_h (f_n, f_s) from Eq. (1). $C_m, C_h, C_n,$ and C_s represent the mean concentration for sediment mixture (sink), high mountains, north alluvial fan, and south alluvial fan, respectively. The subscripts of 1 and 2 represent the first and second tracers in three sediment sources and sediment mixture. $\sigma_m^2, \sigma_h^2, \sigma_n^2,$ and σ_s^2 are the variances of the mean concentrations for the sediment mixture, high mountains, north alluvial fan, and south alluvial fan. In reality, two tracers from the same source/sink samples may not be independent of each other. Therefore, covariance terms should be used to account for this (Phillips and Gregg 2001):

$$\begin{aligned} \sigma_{f_h}' = & \sigma_{f_h}^2 + 2 \frac{\partial f_h}{\partial C_{m_1}} \frac{\partial f_h}{\partial C_{m_2}} \rho_{C_{m_1} C_{m_2}} \sigma_{C_{m_1}} \sigma_{C_{m_2}} + 2 \frac{\partial f_h}{\partial C_{h_1}} \frac{\partial f_h}{\partial C_{h_2}} \rho_{C_{h_1} C_{h_2}} \sigma_{C_{h_1}} \sigma_{C_{h_2}} \\ & + 2 \frac{\partial f_h}{\partial C_{n_1}} \frac{\partial f_h}{\partial C_{n_2}} \rho_{C_{n_1} C_{n_2}} \sigma_{C_{n_1}} \sigma_{C_{n_2}} + 2 \frac{\partial f_h}{\partial C_{s_1}} \frac{\partial f_h}{\partial C_{s_2}} \rho_{C_{s_1} C_{s_2}} \sigma_{C_{s_1}} \sigma_{C_{s_2}} \end{aligned} \tag{4}$$

where ρ is the correlation coefficients between the two tracers for the three sediment sources and sediment mixture. If the two tracers are independent of each other, then $\sigma_{f_h}' = \sigma_{f_h}^2$, or the variance of f_h is σ_{f_h}' . An approximate 95% confidence intervals (CI) for f_h (the same for f_n and f_s) can be obtained by a t distribution as $f_h \pm t_{0.05, \gamma} \sigma_{f_h}'$, where γ represent the

Satterthwaite approximation for the degrees of freedom associated with $\sigma_{f_h}^2$ (Phillips and Gregg 2001):

$$\gamma = \frac{\left(\sum_i a_i V_i\right)^2}{\sum_i \frac{(a_i V_i)^2}{d_i}} \tag{5}$$

where a_i and V_i are the coefficients and variance from the right of Eqs. (3) and (4) estimated by the average value of tracer concentration, and d_i is the degree of freedom of sample number ($n_i - 1$). An Excel spreadsheet was used to calculated source proportions, standard errors, and 95% CI in this text. The absolute mean relative error (AMRE) of each element pair in any single particle size group was used to assess the results from the mixing model calculations against sampled values, which was calculated using Eq. (5):

$$AMRE = \left| C_i - \frac{\sum_{s=1}^m S_{s,i} P_{as}}{C_i} \right| / C_i \tag{6}$$

where P_{as} is the contribution of s source in each particle size group.

2.5 Tracer screening

The tracer screening process began with the removal of non-conservative tracers according to element concentration. A tracer was considered non-conservative and not used for analysis if an individual or mean concentration of a tracer in a sediment mixtures fell outside of the range between the minimum and maximum concentrations of this tracer in all sources (Wilkinson et al. 2013). The remaining conservative tracers were then tested using the Kruskal–Wallis H test to remove the tracers that could not statistically discriminate among the three sources. For additional screening, the tracer variability ratio was used to remove tracers that have greater variability within sources than between sources (Pulley et al. 2015). The tracer variability ratio was calculated based on the percentage difference of the medians of the tracer concentrations between the two sediment source groups divided by the mean within a source group coefficient of variation (%) for the two source groups. Any tracer with variability ratio less than 1 in any source groups was rejected (Pulley et al. 2015). Finally,

the estimated proportions for each source were calculated using analytical solutions. Any pair of tracers that yielded a negative proportion indicated an obvious error, which could stem from sampling error, chemical analysis error, a certain degree of non-conservativeness, or contradiction between the two tracers; and thus were removed. The remaining tracer pairs with positive solutions were used for obtaining the mean contributions of the three sediment sources.

3 Results

3.1 Proportional contributions in different particle size groups

Out of the original 30 chemical elements and oxide compounds analyzed in the particle size group of < 0.063 mm, there were 10 tracers that passed the range and conservativeness tests, the Kruskal–Wallis H test, and the tracer variability ratio test (Table 2). The remaining 10 tracers produced 19 non-contradictory tracer pairs. These 19 tracer pairs were used to estimate the value of source proportions, standard deviation (SD), lower limit (L), and upper limit (U) of the 95% CI (Table 3). The frequency distributions of the 19 tracer pairs from the particle size group of < 0.063 mm are shown in Fig. 2. The estimated proportions of multiple composite fingerprints varied widely for the three potential sediment sources (0.008 to 0.478 for north alluvial fan, 0.007 to 0.573 for south alluvial fan, and 0.202 to 0.598 for high mountains). However, if the estimated proportions of the three sources from any single tracer pair under a certain particle size group were considered, then the estimated proportions from this tracer pair were not so meaningful. This is demonstrated by the wide 95% CI for the each of 19 pairs were larger, indicating that any estimates of the three sediment sources for the mixed sediment from any tracer pairs were unreliable. The large differences in proportions estimated by each tracer pair are hypothesized to primarily result from the differences between tracers in their analytical errors, sampling errors due to spatiotemporal variation, and degrees of the conservativeness during transport. To reduce estimated uncertainties and average out errors, all tracer pairs that produced positive solutions were used to estimate the average proportions, as well as the 95% CI. The resulting source proportion estimates showed significantly narrower 95% CI, and as a result, were more meaningful. Through the use of the average values of all 19 tracer pairs for estimating source contributions, the accuracy was increased and uncertainty reduced. The results also showed that the number of utilized composite fingerprints is crucial for producing meaningful source contributions. In this particle size group, the overall average proportions (SE) were $35.1\% \pm 0.03$, $25.8\% \pm 0.04$, and $39.1\% \pm 0.03$ for the north alluvial fan, south alluvial fan, and high mountains, respectively (Table 4). The absolute mean relative error (AMRE \pm SD)

calculated with Eq. 5 was approximately $1.3\% \pm 1.0\%$ (Table 5).

For the particle size group of 0.063–0.1 mm, there were 14 tracers that passed the range and conservativeness tests, the Kruskal–Wallis H test, and the tracer variability ratio test (Table 2). The remaining 14 tracers yielded 28 tracer pairs that produced positive solutions or proportions. The frequency distributions of the estimated proportions from the 28 tracer pairs are shown in Fig. 2. The estimated source proportions ranged from 0.055 to 0.424 for the north alluvial fan, from 0.057 to 0.697 for the south alluvial fan, and from 0.248 to 0.684 for the high mountains. In this particle size group (0.063–0.1 mm), the estimated proportion average (\pm SE) for the three sediment sources were $14.2\% \pm 0.02$, $39.5\% \pm 0.03$, and $46.3\% \pm 0.02$ for the north alluvial fan, south alluvial fan, and high mountains, respectively (Table 4), with AMRE being $2.2\% \pm 0.7\%$ (Table 5).

There were 13 tracers that passed all the screening tests in the particle size group of 0.10–0.25 mm (Table 2). The remaining 13 tracers yielded 33 tracer pairs that produced positive solutions for the three sediment sources. The frequency distributions of the estimated proportions from the 33 tracer pairs are shown in Fig. 2. The estimated source proportions ranged from 0.014 to 0.647 for the north alluvial fan, from 0.002 to 0.821 for the south alluvial fan, and from 0.127 to 0.820 for the high mountains. In this particle size group (0.10–0.25 mm), the estimated mean proportions (SE) for the three sediment sources were $29.9\% \pm 0.03$, $22.6\% \pm 0.04$, and $47.5\% \pm 0.03$ for the north alluvial fan, south alluvial fan, and high mountains, respectively (Table 4), with AMRE being $5.2\% \pm 3.4\%$ (Table 5).

There were eight tracers that passed all the screening tests in the particle size group of 0.25–0.5 mm (Table 2), and from those eight tracers, 10 tracer pairs produced positive solutions for the three sediment sources. The frequency distributions of the estimated proportions from the 10 tracer pairs are shown in Fig. 2. The estimated source proportions ranged from 0.007 to 0.300 for the north alluvial fan, from 0.013 to 0.306 for the south alluvial fan, and from 0.395 to 0.813 for the high mountains. In this particle size group (0.25–0.5 mm), the estimated mean proportions (SE) for the three sediment sources were $16.5\% \pm 0.03$, $16.7\% \pm 0.03$, and $66.8\% \pm 0.05$ for the north alluvial fan, south alluvial fan, and high mountains, respectively (Table 4), with AMRE being $3.4\% \pm 2.4\%$ (Table 5).

Only six tracers passed all the screening tests in the particle size group of 0.5–1 mm (Table 2), and seven tracer pairs produced positive solutions for the three sediment sources. The frequency distributions of the estimated proportions from seven tracer pairs are shown in Fig. 2. The estimated source proportions ranged from 0.052 to 0.432 for the north alluvial fan, from 0.070 to 0.462 for the south alluvial fan, and from 0.329 to 0.878 for the high mountains. In this particle size group (0.5–1 mm), the estimated mean proportions (SE) for

Table 2 Mean, standard deviation (SD), tests of normality of tracers, and Kruskal–Wallis *H* test in each particle size group

| Tracer | North alluvial fan | | South alluvial fan | | High mountains | | Sediment mixture | | <i>H</i> test ^a | Tracer |
|--------------------------------|--------------------|----------------|--------------------|----------------|----------------|----------------|------------------|----------------|----------------------------|--------------------------------|
| | Mean ± SD | <i>P</i> value | Mean ± SD | <i>P</i> value | Mean ± SD | <i>P</i> value | Mean ± SD | <i>P</i> value | | |
| <0.063 mm | | | | | | | | | | 0.063–0.1 mm |
| P | 824.0 ± 60.3 | 0.976 | 791.8 ± 210.9 | 0.054 | 1152.0 ± 79.6 | 0.747 | 947.7 ± 72.2 | 0.263 | 0.000 | P |
| Zn | 40.2 ± 4.5 | 0.216 | 48.5 ± 6.6 | 0.637 | 52.9 ± 4.8 | 0.308 | 46.3 ± 4.6 | 0.887 | 0.000 | Mn |
| As | 9.4 ± 0.7 | 0.971 | 11.0 ± 1.6 | 0.232 | 14.8 ± 0.9 | 0.898 | 11.4 ± 0.8 | 0.968 | 0.000 | Cu |
| Rb | 65.2 ± 2.7 | 0.773 | 75.1 ± 5.1 | 0.888 | 82.1 ± 3.1 | 0.961 | 74.1 ± 3.9 | 0.928 | 0.000 | Ga |
| Ba | 424.2 ± 20.9 | 0.481 | 483.3 ± 80.3 | 0.032 | 507.3 ± 19.1 | 0.926 | 493.2 ± 18.2 | 0.996 | 0.000 | As |
| Pb | 13.4 ± 1.6 | 0.317 | 15.0 ± 1.5 | 0.705 | 19.3 ± 1.5 | 0.899 | 16.0 ± 2.1 | 0.981 | 0.000 | Rb |
| Al ₂ O ₃ | 8.5 ± 0.3 | 0.656 | 9.7 ± 0.5 | 0.709 | 10.5 ± 0.4 | 0.372 | 9.5 ± 0.4 | 0.953 | 0.000 | La |
| CaO | 8.8 ± 0.5 | 0.553 | 7.4 ± 0.9 | 0.27 | 6.9 ± 0.2 | 0.997 | 7.0 ± 0.5 | 0.839 | 0.000 | Ce |
| Na ₂ O | 2.3 ± 0.1 | 0.947 | 2.2 ± 0.3 | 0.09 | 2.4 ± 0.1 | 0.953 | 2.4 ± 0.1 | 0.974 | 0.000 | Nd |
| K ₂ O | 1.6 ± 0.1 | 0.76 | 1.8 ± 0.1 | 0.917 | 2.0 ± 0.1 | 0.635 | 1.8 ± 0.1 | 1 | 0.000 | Pb |
| 0.1–0.25 mm | | | | | | | | | | Al ₂ O ₃ |
| P | 478.9 ± 74.8 | 0.551 | 611.9 ± 61.5 | 0.315 | 549.2 ± 33.6 | 0.739 | 486.8 ± 64.5 | 0.858 | 0.000 | CaO |
| Cr | 131.7 ± 106.6 | 0.032 | 131.6 ± 40.8 | 0.385 | 65.6 ± 8.1 | 0.917 | 109.4 ± 44.2 | 0.847 | 0.000 | Na ₂ O |
| Mn | 531.7 ± 83.9 | 0.784 | 698.2 ± 59.9 | 0.222 | 622.9 ± 29.6 | 0.611 | 609.1 ± 71.2 | 0.999 | 0.000 | K ₂ O |
| Ni | 40.5 ± 6.4 | 0.667 | 64.9 ± 19.6 | 0.059 | 29.8 ± 1.7 | 0.661 | 36.8 ± 2.7 | 0.985 | 0.000 | 0.25–0.5 mm |
| Cu | 26.2 ± 4.1 | 0.621 | 33.5 ± 6.6 | 0.043 | 21.7 ± 1.6 | 0.808 | 22.4 ± 3.0 | 0.963 | 0.000 | Ni |
| Ga | 13.2 ± 1.0 | 0.931 | 14.9 ± 0.7 | 0.899 | 15.3 ± 0.4 | 0.866 | 14.6 ± 0.7 | 0.709 | 0.000 | Rb |
| As | 6.5 ± 1.3 | 0.764 | 11.8 ± 5.1 | 0.233 | 8.0 ± 0.7 | 0.715 | 7.1 ± 0.9 | 0.964 | 0.000 | Sr |
| Rb | 78.0 ± 4.5 | 0.874 | 82.0 ± 6.6 | 0.684 | 92.7 ± 1.2 | 0.942 | 83.1 ± 6.4 | 1 | 0.000 | Ba |
| SiO ₂ | 55.9 ± 5.0 | 0.287 | 55.4 ± 3.1 | 0.567 | 60.4 ± 0.6 | 0.982 | 58.7 ± 2.0 | 0.763 | 0.003 | Pb |
| Al ₂ O ₃ | 10.0 ± 0.5 | 0.57 | 10.9 ± 0.3 | 0.795 | 11.6 ± 0.1 | 0.999 | 10.8 ± 0.1 | 0.443 | 0.000 | SiO ₂ |
| MgO | 3.0 ± 0.7 | 0.192 | 3.0 ± 0.6 | 0.871 | 2.1 ± 0.1 | 0.779 | 2.4 ± 0.3 | 0.979 | 0.004 | MgO |
| CaO | 7.6 ± 1.6 | 0.286 | 5.5 ± 0.6 | 0.345 | 4.8 ± 0.1 | 0.935 | 5.6 ± 0.7 | 0.975 | 0.000 | K ₂ O |
| Na ₂ O | 2.6 ± 0.3 | 0.375 | 3.0 ± 0.8 | 0.001 | 3.2 ± 0.1 | 0.947 | 3.1 ± 0.1 | 0.747 | 0.000 | 1–2 mm |
| 0.5–1 mm | | | | | | | | | | Cr |
| Ga | 13.4 ± 1.6 | 0.837 | 15.1 ± 0.8 | 0.391 | 14.4 ± 0.5 | 0.94 | 14.4 ± 0.6 | 0.981 | 0.000 | Mn |
| Rb | 78.8 ± 10.0 | 0.042 | 78.5 ± 4.2 | 0.728 | 91.8 ± 2.3 | 0.93 | 83.0 ± 2.5 | 0.999 | 0.000 | Cu |
| Ba | 841.9 ± 216.7 | 0.663 | 583.6 ± 176.8 | 0.199 | 685.3 ± 25.0 | 0.694 | 728.5 ± 24.3 | 0.586 | 0.000 | Ga |
| SiO ₂ | 53.7 ± 2.2 | 0.943 | 56.8 ± 62.2 | 0.61 | 62.2 ± 0.7 | 0.992 | 61.4 ± 1.3 | 0.755 | 0.000 | Rb |
| MgO | 3.3 ± 0.4 | 0.994 | 3.1 ± 1.9 | 0.349 | 1.9 ± 0.1 | 0.983 | 2.3 ± 0.2 | 0.676 | 0.000 | Zr |
| CaO | 7.6 ± 1.9 | 0.792 | 4.4 ± 0.4 | 0.794 | 4.9 ± 0.2 | 0.881 | 5.2 ± 0.5 | 0.629 | 0.000 | Ba |
| | | | | | | | | | | Nd |
| | | | | | | | | | | SiO ₂ |
| | | | | | | | | | | Fe ₂ O ₃ |
| | | | | | | | | | | CaO |
| | | | | | | | | | | Na ₂ O |
| North alluvial fan | | | | | | | | | | <i>H</i> test ^a |
| Mean ± SD | | <i>P</i> value | Mean ± SD | <i>P</i> value | Mean ± SD | <i>P</i> value | Mean ± SD | <i>P</i> value | | |
| 0.063–0.1 mm | | | | | | | | | | |
| 442.7 ± 64.5 | 0.944 | | 562.9 ± 129.3 | 0.638 | 699.3 ± 67.9 | 0.839 | 590.0 ± 73.8 | 0.998 | | 0.000 |

Table 2 (continued)

| | | | | | | | | |
|---------------|-------|---------------|-------|--------------|-------|--------------|-------|-------|
| 452.5 ± 40.5 | 0.754 | 559.4 ± 108.1 | 0.365 | 622.6 ± 10.5 | 0.879 | 588.7 ± 49.2 | 0.258 | 0.000 |
| 18.9 ± 2.0 | 0.908 | 25.8 ± 3.3 | 0.438 | 22.3 ± 0.8 | 0.89 | 23.8 ± 2.3 | 0.899 | 0.000 |
| 10.9 ± 0.6 | 0.982 | 12.4 ± 1.1 | 0.414 | 14.0 ± 0.7 | 0.959 | 13.2 ± 0.4 | 0.99 | 0.000 |
| 6.3 ± 0.9 | 0.878 | 9.3 ± 1.6 | 0.324 | 10.4 ± 1.0 | 0.98 | 9.6 ± 0.9 | 0.961 | 0.000 |
| 63.9 ± 3.5 | 0.915 | 73.4 ± 3.9 | 0.532 | 85.5 ± 2.1 | 0.627 | 75.4 ± 3.3 | 0.954 | 0.000 |
| 21.1 ± 4.2 | 0.979 | 28.5 ± 4.1 | 0.584 | 35.2 ± 3.8 | 0.921 | 34.4 ± 8.1 | 0.87 | 0.000 |
| 50.8 ± 8.1 | 0.519 | 60.6 ± 10.4 | 0.951 | 70.5 ± 8.5 | 0.985 | 70.5 ± 16.9 | 0.706 | 0.000 |
| 14.2 ± 3.8 | 0.944 | 17.8 ± 4.8 | 0.517 | 23.2 ± 2.2 | 0.933 | 19.4 ± 4.8 | 0.648 | 0.000 |
| 14.4 ± 1.1 | 0.917 | 15.6 ± 1.3 | 0.938 | 19.4 ± 1.1 | 0.987 | 17.7 ± 1.4 | 0.902 | 0.000 |
| 8.3 ± 0.3 | 0.914 | 9.1 ± 0.5 | 0.346 | 10.7 ± 0.2 | 0.675 | 9.6 ± 0.2 | 0.64 | 0.000 |
| 7.0 ± 0.7 | 0.408 | 5.9 ± 1.1 | 0.761 | 5.2 ± 0.4 | 0.388 | 5.7 ± 0.4 | 0.751 | 0.000 |
| 2.3 ± 0.0 | 0.923 | 2.4 ± 0.4 | 0.318 | 2.7 ± 0.1 | 0.947 | 2.5 ± 0.1 | 0.983 | 0.000 |
| 1.7 ± 0.1 | 0.997 | 1.8 ± 0.1 | 0.989 | 2.2 ± 0.1 | 0.741 | 1.9 ± 0.1 | 0.961 | 0.000 |
| 0.25–0.5 mm | | | | | | | | |
| 44.6 ± 5.9 | 0.742 | 65.1 ± 24.3 | 0.012 | 27.5 ± 1.4 | 0.992 | 33.1 ± 6.3 | 0.449 | 0.000 |
| 79.9 ± 7.4 | 0.121 | 80.3 ± 4.8 | 0.127 | 91.4 ± 1.7 | 0.678 | 88.6 ± 3.8 | 0.609 | 0.000 |
| 277.0 ± 45.4 | 0.494 | 232.2 ± 42.4 | 0.131 | 315.4 ± 6.3 | 0.755 | 309.4 ± 16.2 | 0.968 | 0.000 |
| 800.9 ± 208.5 | 0.347 | 631.4 ± 151.2 | 0.557 | 663.2 ± 15.2 | 0.999 | 694.6 ± 34.3 | 0.989 | 0.025 |
| 17.4 ± 1.8 | 0.705 | 14.2 ± 2.1 | 0.654 | 16.7 ± 0.4 | 0.866 | 16.1 ± 1.4 | 0.663 | 0.000 |
| 54.5 ± 1.3 | 0.949 | 56.8 ± 3.6 | 0.154 | 62.6 ± 0.7 | 0.516 | 61.2 ± 1.3 | 0.876 | 0.000 |
| 3.2 ± 0.3 | 0.379 | 2.9 ± 0.7 | 0.425 | 1.8 ± 0.1 | 0.705 | 2.0 ± 0.2 | 0.919 | 0.000 |
| 2.2 ± 0.3 | 0.65 | 2.0 ± 0.1 | 0.185 | 2.3 ± 0.1 | 0.992 | 2.2 ± 0.1 | 0.933 | 0.000 |
| 1–2 mm | | | | | | | | |
| 70.3 ± 28.5 | 0.307 | 118.3 ± 36.4 | 0.327 | 51.5 ± 7.0 | 0.875 | 58.8 ± 7.0 | 0.705 | 0.000 |
| 662.4 ± 89.6 | 0.466 | 863.9 ± 179.8 | 0.352 | 563.3 ± 23.9 | 0.877 | 625.5 ± 29.2 | 0.906 | 0.000 |
| 27.5 ± 4.6 | 0.296 | 34.6 ± 9.3 | 0.12 | 16.9 ± 0.7 | 0.928 | 22.0 ± 1.3 | 0.627 | 0.000 |
| 13.3 ± 1.7 | 0.816 | 15.3 ± 0.9 | 0.998 | 13.7 ± 0.5 | 0.74 | 14.7 ± 0.7 | 0.823 | 0.000 |
| 75.8 ± 12.3 | 0.051 | 73.5 ± 4.8 | 0.912 | 84.1 ± 3.6 | 0.759 | 81.3 ± 2.0 | 0.979 | 0.003 |
| 127.0 ± 23.0 | 0.901 | 111.6 ± 15.0 | 0.299 | 89.9 ± 8.6 | 0.959 | 107.4 ± 7.0 | 0.435 | 0.000 |
| 853.7 ± 240.9 | 0.799 | 561.6 ± 201.9 | 0.271 | 669.7 ± 39.1 | 0.83 | 759.4 ± 26.1 | 0.902 | 0.000 |
| 19.9 ± 5.9 | 0.949 | 15.1 ± 3.9 | 0.956 | 11.3 ± 1.4 | 0.993 | 13.4 ± 2.7 | 0.986 | 0.001 |
| 53.8 ± 2.8 | 0.851 | 56.7 ± 3.2 | 0.897 | 61.1 ± 0.9 | 0.855 | 57.7 ± 1.0 | 0.999 | 0.000 |
| 4.6 ± 0.7 | 0.496 | 6.1 ± 1.4 | 0.151 | 3.3 ± 0.3 | 0.997 | 4.1 ± 0.2 | 0.703 | 0.000 |
| 7.9 ± 2.4 | 0.267 | 4.3 ± 0.7 | 0.894 | 5.9 ± 0.4 | 0.602 | 5.8 ± 0.3 | 0.888 | 0.000 |
| 3.6 ± 0.4 | 0.74 | 3.0 ± 0.3 | 0.626 | 3.3 ± 0.1 | 0.867 | 3.6 ± 0.1 | 0.874 | 0.000 |

Note: *P* value > 0.05 indicates that a normal distribution of tracer concentrations cannot be rejected

^a Significance probability of the Kruskal–Wallis test

Table 3 Estimated proportions (EP, %), standard deviation (SD), lower limit (L), and upper limit (U) of the 95% confidence intervals for three sources from each tracer (only listing the particle size group of <0.063 mm)

| Tracer pair | | North alluvial fan | | | | South alluvial fan | | | | High mountains | | | |
|--------------------------------|--------------------------------|--------------------|------|------|------|--------------------|------|------|------|----------------|------|------|------|
| | | EP | SD | 95L | 95U | EP | SD | 95L | 95U | EP | SD | 95L | 95U |
| Na ₂ O | Rb | 47.2 | 0.15 | 0.16 | 0.79 | 0.7 | 0.21 | 0.00 | 0.46 | 52.1 | 0.11 | 0.28 | 0.77 |
| Al ₂ O ₃ | Na ₂ O | 46.6 | 0.12 | 0.20 | 0.73 | 1.2 | 0.18 | 0.00 | 0.41 | 52.2 | 0.11 | 0.28 | 0.76 |
| K ₂ O | Na ₂ O | 45.8 | 0.15 | 0.13 | 0.78 | 1.8 | 0.21 | 0.00 | 0.47 | 52.4 | 0.11 | 0.28 | 0.77 |
| Pb | Zn | 47.8 | 0.35 | 0.00 | 1.00 | 11.8 | 0.64 | 0.00 | 1.00 | 40.4 | 0.29 | 0.00 | 1.00 |
| Al ₂ O ₃ | Rb | 42.3 | 1.80 | 0.00 | 1.00 | 12.4 | 4.54 | 0.00 | 1.00 | 45.2 | 2.74 | 0.00 | 1.00 |
| Zn | P | 47.1 | 0.20 | 0.03 | 0.91 | 13.9 | 0.21 | 0.00 | 0.58 | 39.1 | 0.07 | 0.23 | 0.55 |
| Pb | P | 44.8 | 0.31 | 0.00 | 1.00 | 15.9 | 0.28 | 0.00 | 0.94 | 39.3 | 0.05 | 0.26 | 0.52 |
| Al ₂ O ₃ | P | 39.0 | 0.12 | 0.13 | 0.65 | 21.2 | 0.14 | 0.00 | 0.51 | 39.8 | 0.07 | 0.24 | 0.56 |
| Rb | P | 38.5 | 0.12 | 0.10 | 0.67 | 21.6 | 0.13 | 0.00 | 0.53 | 39.8 | 0.07 | 0.24 | 0.55 |
| K ₂ O | P | 36.8 | 0.13 | 0.07 | 0.67 | 23.2 | 0.14 | 0.00 | 0.55 | 40.0 | 0.07 | 0.25 | 0.55 |
| Pb | Al ₂ O ₃ | 36.8 | 0.29 | 0.00 | 0.94 | 27.0 | 0.56 | 0.00 | 1.00 | 36.2 | 0.28 | 0.00 | 0.94 |
| Rb | Pb | 35.6 | 0.35 | 0.00 | 1.00 | 28.7 | 0.65 | 0.00 | 1.00 | 35.7 | 0.30 | 0.00 | 0.98 |
| As | Zn | 41.0 | 0.27 | 0.00 | 0.99 | 31.3 | 0.40 | 0.00 | 1.00 | 27.7 | 0.15 | 0.00 | 0.58 |
| Pb | K ₂ O | 33.0 | 0.36 | 0.00 | 1.00 | 32.3 | 0.67 | 0.00 | 1.00 | 34.7 | 0.31 | 0.00 | 0.98 |
| Na ₂ O | Ba | 7.5 | 0.15 | 0.00 | 0.39 | 32.7 | 0.23 | 0.00 | 0.79 | 59.8 | 0.14 | 0.31 | 0.89 |
| As | Al ₂ O ₃ | 28.6 | 0.19 | 0.00 | 0.69 | 48.8 | 0.32 | 0.00 | 1.00 | 22.6 | 0.14 | 0.00 | 0.51 |
| Rb | As | 25.5 | 0.24 | 0.00 | 0.75 | 53.2 | 0.39 | 0.00 | 1.00 | 21.4 | 0.16 | 0.00 | 0.54 |
| P | Ba | 0.8 | 0.20 | 0.00 | 0.41 | 56.0 | 0.26 | 0.05 | 1.00 | 43.2 | 0.10 | 0.22 | 0.64 |
| K ₂ O | As | 22.5 | 0.24 | 0.00 | 0.73 | 57.3 | 0.39 | 0.00 | 1.00 | 20.2 | 0.16 | 0.00 | 0.52 |

the three sediment sources were 19.6% ± 0.05, 24.9% ± 0.05, and 55.5% ± 0.09 for the north alluvial fan, south alluvial fan, and high mountains, respectively (Table 4), with AMRE being 3.5% ± 1.4% (Table 5).

There were 12 tracers that passed all screening tests in the particle size group of 1.0–2.0 mm (Table 2), and from those 12 tracers, 29 tracer pairs produced positive solutions for the three sediment sources. The frequency distributions of the

Fig. 2 Relative frequency distributions of the mean proportional contributions from the north alluvial fan, south alluvial fan, and high mountains, estimated using multiple composite fingerprints for the six particle size groups

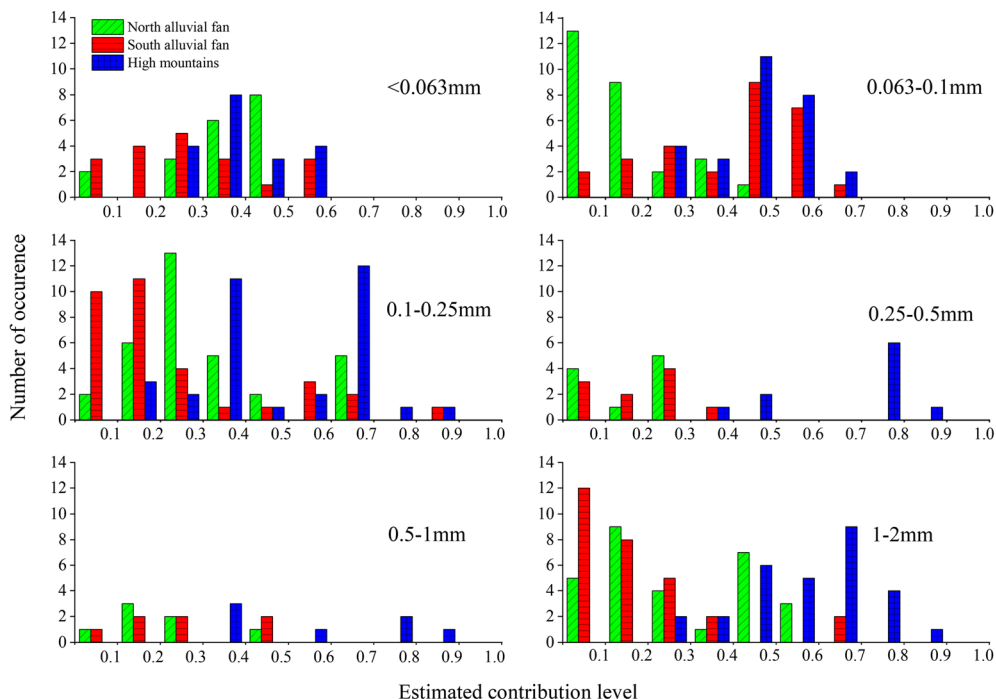


Table 4 Estimated proportion (EP, %) using the means of multiple composite fingerprints, standard error (SE), lower limit (L), upper limit (U) of the 95% confidence intervals, and the number of tracer pairs (NTP) for six particle size groups

| Size (mm) | North alluvial fan | | | | South alluvial fan | | | | High mountains | | | | NTP |
|-----------|--------------------|------|------|------|--------------------|------|------|------|----------------|------|------|------|-----|
| | EP | SE | 95L | 95U | EP | SE | 95L | 95U | EP | SE | 95L | 95U | |
| < 0.063 | 35.1 | 0.03 | 0.29 | 0.41 | 25.8 | 0.04 | 0.18 | 0.34 | 39.1 | 0.03 | 0.34 | 0.44 | 19 |
| 0.063–0.1 | 14.2 | 0.02 | 0.10 | 0.19 | 39.5 | 0.03 | 0.33 | 0.46 | 46.3 | 0.02 | 0.42 | 0.50 | 28 |
| 0.1–0.25 | 29.9 | 0.03 | 0.24 | 0.36 | 22.6 | 0.04 | 0.15 | 0.30 | 47.5 | 0.03 | 0.41 | 0.54 | 33 |
| 0.25–0.5 | 16.5 | 0.03 | 0.10 | 0.23 | 16.7 | 0.03 | 0.10 | 0.23 | 66.8 | 0.05 | 0.57 | 0.76 | 10 |
| 0.5–1 | 19.6 | 0.05 | 0.10 | 0.29 | 24.9 | 0.05 | 0.14 | 0.35 | 55.5 | 0.09 | 0.39 | 0.72 | 7 |
| 1–2 | 26.3 | 0.03 | 0.20 | 0.32 | 17.0 | 0.03 | 0.11 | 0.23 | 56.7 | 0.03 | 0.51 | 0.62 | 29 |

estimated proportions from 29 tracer pairs are shown in Fig. 2. The estimated source proportions ranged from 0.018 to 0.567 for the north alluvial fan, from 0.004 to 0.632 for the south alluvial fan, and from 0.266 to 0.878 for the high mountains. In this particle size group (1.0–2.0 mm), the estimated mean proportions (SE) for the three sediment sources were $26.3\% \pm 0.03$, $17.0\% \pm 0.03$, and $56.7\% \pm 0.03$ for the north alluvial fan, south alluvial fan, and high mountains, respectively (Table 4), with AMRE being $4.0\% \pm 2.0\%$ (Table 5).

3.2 Contributions of different sediment sources

In order to determine the contributions of the three potential sediment sources to the downstream sediment mixtures, the estimated proportions of each particle size group from each source were multiplied by the mass fraction of the sediment in the corresponding mixed sediment size groups (Table 5). The results showed that the contributions of the three sediment sources to the mixed sediment were 24.5% for the north alluvial fan, 26.5% for the south alluvial fan, and 49.0% for the high mountains during the duration of this investigation. The total estimation error was approximately 3.5%. The contributions from each individual size group were also presented. The 0.10–0.25 mm particle size group produced the largest mass percentage and accounted for 27.1% of the mixed sediment, of which 8.1%, 6.1%, and 12.9% were the contributions from the north alluvial fan, south alluvial fan, and high mountains, respectively. On the contrary, the 1.0–2.0 mm particle size group produced the smallest mass percentage and only accounted for 0.7% of the mixed sediment, of which 0.2%, 0.1%, and 0.4% were the contributions from the north alluvial fan, south alluvial fan, and high mountains, respectively. Consequently, with less than 1% of the largest particle size group being represented in the mixed sediment, this indicates that the 1.0–2.0 mm particles were too coarse to be transported by the runoff events which occurred during the duration of this investigation.

3.3 Uncertainty of mean contributions

The uncertainty contributions of the estimated source proportions for the three sources were calculated using Eqs. (3) and (4). The relative uncertainty contributions of the three sources and sediment mixture for the variation of f_h (the same for f_n and f_s) were estimated by dividing the respective terms on the right hand side of Eq. (4) by $\sigma_{f_h}^2$ (Table 6). Overall, compared with the uncertainty contributions from each source, the uncertainty contributions from the sediment mixture accounted for the majority of the total uncertainty. The overall averaged uncertainty contributions from the sediment mixture to the estimated proportions of the three sources were 65.8%, 67.6%, and 66.8% for the north alluvial fan, south alluvial fan, and high mountains, respectively. Correspondingly, the overall averaged uncertainty contributions from the north alluvial fan to the proportions of the three sediment sources were 14.4%, 13.0%, and 12.5%, from the high mountains were 11.1%, 10.4%, and 11.6%, and from the south alluvial fan were 8.7%, 9.1%, and 9.1% for the north alluvial fan, south alluvial fan, and high mountains, respectively.

4 Discussion

Compared with a mean, a median is less sensitive to extreme values for a skewed distribution. If the extreme values are outliers, the median is preferred to the mean to minimize error. Otherwise, the mean may be preferred to give more weights to the extreme values. In this study, we tested the contributions of three sources based on the means and medians of multiple composite fingerprints for six particle size groups, and the results indicated that there were little differences between the means and medians of multiple composite fingerprints except for a few individual cases, and but the order of contributions of three sources was the same between the means and medians in six particle size groups. We also found that the sum of the contributions of three sources from

Table 5 Mean source contributions estimated using multiple composite fingerprints for three sources (NAF = north alluvial fan, SAF = south alluvial fan, HM = high mountains, and SM = sediment mixture)

| Size (mm) | Mean proportion (%) | | | Size distribution of SM (%) | Contribution of each particle size (%) | | | AMRE \pm SD (%) |
|-----------|---------------------|------|------|-----------------------------|--|------|------|-------------------|
| | NAF | SAF | HM | | NAF | SAF | HM | |
| < 0.063 | 35.1 | 25.8 | 39.1 | 25.2 | 8.9 | 6.5 | 9.8 | 1.3 \pm 1.0 |
| 0.063–0.1 | 14.2 | 39.5 | 46.3 | 23.5 | 3.3 | 9.3 | 10.9 | 2.2 \pm 0.7 |
| 0.1–0.25 | 29.9 | 22.6 | 47.5 | 27.1 | 8.1 | 6.1 | 12.9 | 5.2 \pm 3.4 |
| 0.25–0.5 | 16.5 | 16.7 | 66.8 | 16.9 | 2.8 | 2.3 | 11.3 | 3.4 \pm 2.4 |
| 0.5–1 | 19.6 | 24.9 | 55.5 | 6.6 | 1.3 | 1.7 | 3.7 | 3.5 \pm 1.4 |
| 1–2 | 26.3 | 17.0 | 56.7 | 0.7 | 0.2 | 0.1 | 0.4 | 4.0 \pm 2.0 |
| Total | | | | 100 | 24.5 | 26.5 | 49.0 | 3.5 |

the medians of multiple composite fingerprints does not equal to 1 or 100% for each of the six particle size groups, varying from 86 to 113% (Table 7). That is to say that the solutions using medians instead of means are not closed. If the medians are used, we would underestimate contributions by as much as 14% or overestimate contributions by 13%. Such errors would be avoided if the means are used.

The results showed that the high mountains consistently contributed more sediment to the downstream sediment mixture than either the north or south alluvial fan for all six particle size categories. The estimated proportions from the high mountains were significantly higher than the other two sources, as illustrated by the non-overlapping 95% CIs in Table 4. This consistency suggests the multiple particle size tracking method used in this investigation worked well under

the boundary conditions and has great potential in minimizing errors in proportion estimation resulting from the non-conservativeness of tracers caused by particle sorting and enrichment of fines during sediment transport. The contributions between the north and south alluvial fans were overall comparable for all six particle size groups, and were not statistically different, likely resulting from their similar topographies and proximities to the sediment sampling location (sink).

The high mountain area accounts for 93.7% of the research area that expectedly had the largest contributing proportion of downstream sediment mixture, which was nearly 49% during the duration of this investigation. The high percentage of sediment is likely a combination of several factors, including the high mountain extreme relief, steeper channel slope, greater orographic effects, and more precipitation compared to the

Table 6 Percent uncertainty contributions from north alluvial fan, south alluvial fan, high mountains, and sediment mixture towards the total uncertainty of the north alluvial fan, south alluvial fan, and high mountains proportion estimates for each particle size group

| Source | Size (mm) | North alluvial fan | South alluvial fan | High mountains | Sediment mixture |
|--------|-----------|--------------------|--------------------|----------------|------------------|
| NAF | < 0.063 | 3.1 | 8.6 | 9.1 | 79.1 |
| | 0.063–0.1 | 0.9 | 15.9 | 9.3 | 73.8 |
| | 0.1–0.25 | 14.6 | 10.8 | 5.4 | 69.2 |
| | 0.25–0.5 | 20.2 | 6.5 | 12.5 | 60.8 |
| | 0.5–1 | 18.8 | 2.8 | 13.3 | 65.1 |
| | 1–2 | 27.3 | 6.7 | 20.8 | 45.3 |
| SAF | < 0.063 | 3.3 | 9.7 | 8.9 | 78.2 |
| | 0.063–0.1 | 0.8 | 16.8 | 7.9 | 74.5 |
| | 0.1–0.25 | 16.8 | 8.2 | 4.8 | 70.2 |
| | 0.25–0.5 | 9.9 | 3.7 | 9.1 | 77.3 |
| | 0.5–1 | 17.2 | 8.5 | 16.0 | 58.2 |
| | 1–2 | 29.2 | 7.2 | 20.0 | 43.6 |
| HM | < 0.063 | 3.2 | 10.3 | 10.1 | 76.4 |
| | 0.063–0.1 | 0.8 | 20.1 | 9.1 | 69.9 |
| | 0.1–0.25 | 14.8 | 4.7 | 3.7 | 76.7 |
| | 0.25–0.5 | 13.3 | 5.3 | 14.9 | 66.4 |
| | 0.5–1 | 15.8 | 4.7 | 15.2 | 64.3 |
| | 1–2 | 26.0 | 9.0 | 19.8 | 45.3 |

Table 7 The estimated contributions of three sources using the medians of multiple composite fingerprints for six particle size groups

| Size (mm) | North alluvial fan (%) | South alluvial fan (%) | High mountains (%) | Total of three sources (%) |
|-----------|------------------------|------------------------|--------------------|----------------------------|
| < 0.063 | 38.5 | 23.2 | 39.8 | 101.5 |
| 0.063–0.1 | 11.1 | 44.1 | 47.9 | 103.1 |
| 0.1–0.25 | 25.0 | 13.9 | 46.7 | 85.6 |
| 0.25–0.5 | 20.3 | 17.6 | 75.1 | 112.9 |
| 0.5–1 | 16.6 | 24.0 | 57.8 | 98.4 |
| 1–2 | 22.4 | 11.3 | 59.6 | 93.3 |

piedmont fans, and subsequent flash flooding. Collectively, a larger amount of high mountain sediment can be conveyed into the lower reaches of the river system during runoff events.

Compared with the high mountains, the alluvial fans on both sides of the river have much smaller drainage areas and less rainfall, but their total contribution of sediment is slightly larger than the high mountains. These results are attributed to (1) alluvial fan surface materials being finer and less consolidated than those in the mountains, which are easier to transport by surface runoff; and (2) transport distances to the mixed sediment sampling location from the fans are significantly shorter than from the high mountains, giving rise to greater sediment transport efficiency for eroded materials from the fans than from the high mountains.

Considering only the piedmont fans, the north alluvial fan has a larger drainage area and more anthropogenic disturbances, yet produced less sediment yield. The estimated contribution of the south alluvial fan is being slightly larger than that of the north alluvial fan. This may be explained by the geology of both alluvial fans. Specifically, in the north alluvial fan, the surface is mainly exposed rocks, and is not easy to erode and weather. In contrast, the south alluvial fan surface materials are mainly a composite of orange-red clastic rocks, and are easily weathered, eroded, and transported, indicating that the type of surface materials played an important role in providing an ample source of sediments for erosional transport.

In Section 3.3, these results revealed that the sediment mixture contributed the largest portion of uncertainty compared to the estimates of the three sediment source proportions. This can be explained as follows. First, each sediment source area is relatively uniform in geology and geomorphology with comparatively smaller spatial variation than the entire study watershed, while the downstream sediment sampling points (sink) incorporate the three sediment source areas and inherit greater spatial variation. Second, the research area is large, and most of the area is not easily accessible. It is possible that the collected samples do not fully represent the sediment properties of the sources, resulting in underestimation of the within source variability. Third, the sediment in each source area is transported to the sediment sink area, and there may be chemical transformations between elements during the transport.

These would increase variability in sediment properties measured at the sink area.

The temporal variability should be further stressed and discussed. Because of spatial variations in storm patterns, storm centers, erosion processes, and rates, variation of collected sediment tends to change with seasons and storm sizes, adding additional temporal variation on top of the already large spatial variation. Therefore, there are greater temporal and spatial variations in the entire watershed than any other potential singular sediment source, which generates large uncertainty (Zhang et al. 2016b). This result suggests that a greater number of samples should be taken for sediment mixtures than for each source to combat the augmented spatial and temporal variations in order to increase the accuracy of the source proportion estimation and minimize the uncertainty caused by the above possible reasons.

5 Conclusions

From a statistical point of view, the estimated contributions of the three sediment sources from any single composite fingerprint were unreliable because of sampling errors, chemical analysis errors, and degree of conservativeness varied with each tracer. The proportional contributions from each sediment source estimated with different composite fingerprints varied considerably, and the 95% CIs of the predicted proportions were quite wide.

To improve the accuracy of estimated mean contributions, all multiple composite fingerprints were averaged to produce relative narrow 95% CIs. During the duration of this investigation, the overall averaged sediment contributions were 49.0%, 26.5%, and 24.5% from the high mountains, south alluvial fan, and north alluvial fan, respectively. The total mean absolute relative error was 3.5%, indicating the multiple composite fingerprinting method can greatly improve the accuracy of sediment contribution estimates. The results also showed using multiple particle size groups has significant potential with regard to increasing the accuracy of proportion estimation, especially when sediment sorting and enrichment of fines are of concern. The proportional contributions from the high mountains were largest for each particle size group,

showing the consistency among multiple size tracking under the study conditions and the potential of overcoming tracer non-conservativeness due to sediment sorting.

The Gaussian first-order approximation showed that the overall uncertainty contribution was more than 60% from the sediment mixture, while less than 15% from any of the three individual sediment sources. This result indicates that a larger sample size for sediment mixture, compared with that of each source, is generally needed to minimize uncertainty of the proportion estimates. The larger uncertainty for the sediment mixture is a byproduct of the sediment sampling location (sink), which inherits both spatial and temporal variations from all contributing sources. The uncertainty contributions are additionally compounded by temporal variations resulting from spatial variations of soil erosion rates that vary with storm patterns, storm size, and seasons. In addition, the large uncertainty with sediment mixture may also indicate that samples from sources may not adequately capture the range of the sediment properties of the sources, or that sediment may undergo geochemical alternation within channels during transport. This conclusion needs to be further examined under different climates and geographic conditions where different erosion and sediment transport processes prevail.

Acknowledgments We thank Mrs. Caixia Zhang for her help in carrying out the elemental analysis, and thank the Technology Service Center of CAREERI, the Chinese Academy of Sciences (CAS) for the sample testing service. Meanwhile, we also thank CSC for supporting this paper. The study was supported by the National Science Fund of China (41501008 and 41701008), the “Light of West China” Program of the CAS, the Science and Technology Program of Gansu Province (17JR5RA303), the Youth Innovation Promotion Association of the CAS (2016373), and technology Research and Development Program of China Railway Corporation (2017G004-E).

References

- Bak L, Michalik A, Tekielak T (2013) The relationship between bank erosion, local aggradation and sediment transport in a small Carpathian stream. *Geomorphology* 191:51–63
- Barker R, Dixon L, Hooke J (1997) Use of terrestrial photogrammetry for monitoring and measuring bank erosion. *Earth Surf Process Landf* 22:1217–1227
- Boardman J, Favis-ortlock D, Foster I (2015) A 13-year record of erosion on badland sites in the Karoo, South Africa. *Earth Surf Process Landf* 40:1964–1981
- Cao YZ, Coote DR (1993) Topography and water erosion in northern Shaanxi Province, China. *Geoderma* 59:249–262
- Collins AL, Walling DE, Leeks GJL (1996) Composite fingerprinting of the spatial source of fluvial suspended sediment: a case study of the Exe and Severn river basins, United Kingdom. *Geomorphol Relief Process Environ* 2:41–53
- Collins AL, Walling DE, Leeks G (1997) Source type ascription for fluvial suspended sediment based on a quantitative composite fingerprinting technique. *Catena* 29:1–27
- Collins AL, Walling DE, Leeks GJL (1998) Use of composite fingerprints to determine the spatial provenance of the contemporary suspended sediment load transported by rivers. *Earth Surf Process Landf* 23:31–52
- Collins AL, Walling DE, Webb L, King P (2010) Apportioning catchment scale sediment sources using a modified composite fingerprinting technique incorporating property weightings and prior information. *Geoderma* 155:249–261
- Collins AL, Pulley S, Foster ID, Gellis A, Porto P, Horowitz AJ (2017) Sediment source fingerprinting as an aid to catchment management: a review of the current state of knowledge and a methodological decision-tree for end-users. *J Environ Manag* 194:86–108
- Davis RJ, Gregory KJ (1994) A new distinct mechanism of river bank erosion in a forested catchment. *J Hydrol* 157:1–11
- Devereux OH, Prestegard KL, Needelman BA, Gellis AC (2010) Suspended-sediment sources in an urban watershed, Northeast Branch Anacostia River, Maryland. *Hydrol Process* 24:1391–1403
- Emamgholizadeh S, Bateni SM, Nielson JR (2018) Evaluation of different strategies for management of reservoir sedimentation in semi-arid regions: a case study (Dez Reservoir). *Lake Reservoir Manag* 34:270–282
- Evrard O, Poulenard J, Nemery J, Ayrault S, Gratiot N, Duvert C, Prat C, Lefevre I, Bonte P, Esteves M (2013) Tracing sediment sources in a tropical highland catchment of central Mexico by using conventional and alternative fingerprinting methods. *Hydrol Process* 27:911–922
- Gingele FX, Deckker PD (2005) Clay mineral, geochemical and Sr-Nd isotopic fingerprinting of sediments in the Murray-Darling fluvial system, southeast Australia. *J Geol Soc Aust* 52:965–974
- Gonzalez JM (2018) Runoff and losses of nutrients and herbicides under long-term conservation practices (no-till and crop rotation) in the U.S. Midwest: a variable intensity simulated rainfall approach. *Int Soil Water Conserv Res* 6:265–274
- Haddadchi A, Olley J, Laceby P (2014) Accuracy of mixing models in predicting sediment source contributions. *Sci Total Environ* 497–498:139–152
- Haddadchi A, Olley J, Pietsch T (2015) Quantifying sources of suspended sediment in three size fractions. *J Soils Sediments* 15:2086–2100
- Hancock GJ, Revill AT (2013) Erosion source discrimination in a rural Australian catchment using compound-specific isotope analysis (CSIA). *Hydrol Process* 27:923–932
- Khaba L, Griffiths JA (2017) Calculation of reservoir capacity loss due to sediment deposition in the Muela reservoir, Northern Lesotho. *Int Soil Water Conserv Res* 5:130–140
- Koiter AJ, Owens PN, Petticrew EL, Lobb DA (2013) The behavioural characteristics of sediment properties and their implications for sediment fingerprinting as an approach for identifying sediment sources in river basins. *Earth-Sci Rev* 125:24–42
- Koiter AJ, Owens PN, Petticrew EL, Lobb DA (2018) Assessment of particle size and organic matter correction factors in sediment source fingerprinting investigations: an example of two contrasting watersheds in Canada. *Geoderma* 325:195–207
- Krause AK, Franks SW, Kalma JD, Loughran RJ, Rowan JS (2003) Multi-parameter fingerprinting of sediment deposition in a small gullied catchment in SE Australia. *Catena* 53:327–348
- Lacey JP, Olley J (2015) An examination of geochemical modelling approaches to tracing sediment sources incorporating distribution mixing and elemental correlations. *Hydrol Process* 29:1669–1685
- Lamba J, Karthikeyan KG, Thompson AM (2015) Using radiometric fingerprinting and phosphorus to elucidate sediment transport dynamics in an agricultural watershed. *Hydrol Process* 29:2681–2693

- Lance JC, McIntyre SC, Naney JW, Rousseva SS (1986) Measuring sediment movement at low erosion rates using cesium-137. *Soil Sci Soc Am J* 50:1303–1309
- Liebe J, van de Giesen N, Andreini M (2005) Estimation of small reservoir storage capacities in a semi-arid environment. *Phys Chem Earth, Parts A/B/C* 30:448–454
- Liu B, Niu Q, Qu J, Zu R (2016) Quantifying the provenance of aeolian sediments using multiple composite fingerprints. *Aeolian Res* 22:117–122
- McKinley R, Radcliffe D, Mukundan R (2013) A streamlined approach for sediment source fingerprinting in a Southern Piedmont watershed, USA. *J Soils Sediments* 13:1754–1769
- Minella JPG, Walling DE, Merten GH (2008) Combining sediment source tracing techniques with traditional monitoring to assess the impact of improved land management on catchment sediment yields. *J Hydrol* 348:546–563
- Motha JA, Wallbrink PJ, Hairsine PB, Grayson RB (2003) Determining the sources of suspended sediment in a forested catchment in south-eastern Australia. *Water Resour Res* 39:53–62
- Nagle GN, Fahey TJ, Ritchie JC, Woodbury PB (2007) Variations in sediment sources and yields in the Finger Lakes and Catskills regions of New York. *Hydrol Process* 21:828–838
- Niu B, Qu J, Zhang X, Liu B, Tan L, An Z (2019) Quantifying provenance of reservoir sediment using multiple composite fingerprints in an arid region experiencing both wind and water erosion. *Geomorphology* 332:112–121
- Olley JM, Murray AS, Mackenzie DH, Edwards K (1993) Identifying sediment sources in a gullied catchment using natural and anthropogenic radioactivity. *Water Resour Res* 29:1037–1043
- Palazon L, Navas A (2017) Variability in source sediment contributions by applying different statistical test for a Pyrenean catchment. *J Environ Manag* 194:42–53
- Phillips DL, Gregg JW (2001) Uncertainty in source partitioning using stable isotopes. *Oecologia* 127:171–179
- Pulley S, Foster I, Antunes P (2015) The uncertainties associated with sediment fingerprinting suspended and recently deposited fluvial sediment in the Nene river basin. *Geomorphology* 228:303–319
- Roo APJD (1991) The use of ¹³⁷Cs as a tracer in an erosion study in south Limburg (the Netherlands) and the influence of Chernobyl fallout. *Hydrol Process* 5:215–227
- Stewart HA, Massoudieh A, Gellis A (2015) Sediment source apportionment in Laurel Hill Creek, PA, using Bayesian chemical mass balance and isotope fingerprinting. *Hydrol Process* 29:2545–2560
- Stone M, Collins AL, Silins U, Emelko MB, Zhang YS (2014) The use of composite fingerprints to quantify sediment sources in a wildfire impacted landscape, Alberta, Canada. *Sci Total Environ* 473–474:642–650
- Thakur PK, Laha C, Aggarwal SP (2012) River bank erosion hazard study of river Ganga, upstream of Farakka barrage using remote sensing and GIS. *Nat Hazards* 61:967–987
- Wallbrink PJ, Olley JM, Hancock GJ (2003) Tracer assessment of catchment sediment contributions to Western Port, Victoria. CSIRO Land and Water technical report 08/03
- Walling DE (2005) Tracing suspended sediment sources in catchments and river systems. *Sci Total Environ* 344:159–184
- Walling DE (2013) The evolution of sediment source fingerprinting investigations in fluvial systems. *J Soils Sediments* 13:1658–1675
- Wilkinson SN, Hancock GJ, Bartley R, Hawdon AA, Keen RJ (2013) Using sediment tracing to assess processes and spatial patterns of erosion in grazed rangelands, Burdekin River basin, Australia. *Agric Ecosyst Environ* 180:90–102
- Zhang XC, Liu BL (2016) Using multiple composite fingerprints to quantify fine sediment source contributions: a new direction. *Geoderma* 268:108–118
- Zhang XC, Liu BL, Liu B, Zhang GH (2016a) Quantifying sediment provenance using multiple composite fingerprints in a small watershed in Oklahoma. *J Environ Qual* 45:1296–1302
- Zhang XC, Zhang GH, Liu BL, Liu B (2016b) Using cesium-137 to quantify sediment source contribution and uncertainty in a small watershed. *Catena* 140:116–124
- Zhang XC, Nearing MA, Garbrecht JD (2017) Gaining insights into interrill soil erosion processes using rare earth element tracers. *Geoderma* 299:63–72
- Zhou H, Chang W, Zhang L (2016) Sediment sources in a small agricultural catchment: a composite fingerprinting approach based on the selection of potential sources. *Geomorphology* 266:11–19

Publisher's note Springer Nature remains neutral with regard to jurisdictional claims in published maps and institutional affiliations.